International Journal of Thermodynamics (IJoT)
ISSN 1301-9724 / e-ISSN 2146-1511
https://dergipark.org.tr/en/pub/ijot

Vol. xx (No. x), pp. xxx-xxx, 2025
doi: 10.5541/ijot.1587174
Published online: Mmm dd, 2025

Research Article

Exergy Analysis of Oxy-Biogas Combustion with Different Rates of the CO_2 Content

[1]*M. Yıldız, [2]S. Özarslan

[1] Iğdır University, Faculty of Engineering, Department of Mechanical Engineering, Iğdır, Türkiye
[2] Amasya University, Technical Sciences Vocational School, Automotive Program, Amasya, Türkiye
E-mail: [1]*melih.yildiz@igdir.edu.tr

Received 18 November 2024, Revised 9 April 2025, Accepted 18 April 2025

Abstract

This work presents the exergetic evaluations of the oxy-biogas combustion process in an adiabatic furnace for the cases of biogas involving different carbon dioxide (CO_2) concentrations. A three-dimensional steady-state computational fluid dynamics model was developed for combustion simulation. The model was first verified with the data of oxy-natural gas and showed good agreement with the data. Thus, simulation studies were performed for the oxy-biogas combustion with different CO_2 concentrations of biogas fuel, from 10 vol% to 40 vol% with a 10% increment, at a constant input power capacity. The results show that the sum of specific thermo-mechanical and chemical exergy of combustion products has a decreasing trend with increasing CO_2 content in biogas. However, the exergy flow rates of the combustion products increased with the increase in CO_2 due to the increasing mass flow rates. Increasing the CO_2 level in biogas led to an increase in the chemical exergy fraction of the combustion products. Thus, the exergy loss fractions resulting from incomplete combustion varied increasingly from 5.8 % to 13.8 % in the range from 10 % CO_2 to 40 % CO_2 contents of biogas.

Keywords: *Biogas; oxy-combustion; chemical exergy; exergy destruction; computational fluid dynamics.*

1. Introduction

The growing global need for energy, the depletion of fossil fuels, and environmental damage have led to increased interest in the use of renewable energy sources. Among green energy sources, biogas is an energy source that can be produced from a wide variety of organic wastes such as municipal waste, agricultural and industrial waste, and sewage sludge. In response to the search for inexhaustible, sustainable, and clean energy, which is one of today's important problems, biogas is a strong candidate because it can be used as a renewable electricity and heat source when needed, stored, and produced from organic waste. Biogas, consisting of combustible methane-CH_4 (50-75%), non-combustible carbon dioxide-CO_2 (25-50%) and small amounts of other gases, and water vapour, is a valuable energy source with a capacity of 5.5-7 kWh m^{-3} [1, 2]. Methane becomes a harmful greenhouse gas when released into the atmosphere, but it directly affects the amount of energy in biogas and is also an important component for reducing harmful emissions and fossil fuel use. For example, it is known that biogas, when used as vehicle fuel, emits less carbon monoxide, hydrocarbon, and nitrogen oxide emissions than gasoline or diesel engines [3].

According to research, the design of the biogas production process and the type of substrate used determine the composition of the gas. Depending on the type of raw material, methane yield varies between 51% and 65%. For example, the methane efficiency of grass silage is 54%, cattle manure is 60%, liquid pig manure is 65%, forage beet is 51%, and corn silage is 52%. However, depending on the feedstock, biogas may contain contaminants including halogenated compounds, sulphur compounds, nitrogen, and organic silicon species [4]. As can be understood, the high and pure methane content of biogas is an important parameter in energy conversion by burning. The methane content determines the calorific value of biogas. The average calorific value of biogas is quite low, at about 21.5 MJ/m^3, compared to the calorific value of natural gas, which is 36 MJ/m^3. By removing non-flammable CO_2 from the biogas composition, higher calorific values of biogas can be obtained when the amount of methane increases [5].

Some cleaning technologies, such as cryogenic process, water cleaning, and membrane, can be used to improve biogas and increase its efficiency. However, gradual clean-up and upgrade processes increase costs. Another solution to improve the biogas combustion process is to reduce CO_2 concentration by blending biogas with different fuels [6, 7]. It is possible to come across examples of blending various fuels and biogas used for this purpose in the literature. Methane, oxygen, propane, hydrogen, microalgae biofuels supported by nanoparticles, and biodiesel are examples of these fuels [8-11].

Another strategy is an oxygen-enriched or oxy-fuel combustion process to improve biogas combustion. Oxygen-enriched biogas combustion has been investigated in the literature, although it is not at a sufficient level. The studies

*Corresponding Author

performed by Yılmaz et al. [12] and Safe et al. [13] show that the stability limits of biogas are improved, and flame temperature increases with oxygen enrichment. In addition to oxygen-enriched and oxy-fuel combustion of biogas, blending of biogas with different fuels under oxygen-enriched and oxy-fuel combustion studies are also available in the literature, such as the use of diesel-biogas blend with oxygen-enriched in an engine [14], biogas/kerosene mixture with oxygen enrichment in a mini gas turbine engine [15], and biogas-propane-oxygen enrichment [16]. In these studies, it was concluded that oxygen enrichment had a significant effect on the entire reaction process and that enrichment of air with O_2 caused an increase in the laminar combustion rates of both fuels examined, respectively. As a summary of the studies in the literature, it was determined that hydrogen addition and oxygen enrichment have positive effects in reducing combustion instability. In biogas combustion studies using hydrogen and oxygen, it was found that CO emissions decreased, and NOx emissions increased with O_2 enrichment, the net heat release rate of the biogas flame increased with the increase in the net reaction rate of the biogas, and more stable combustion was achieved [17-19].

However, the evaluation of these strategies is a critical issue to determine which strategy is more useful and its improvement potential for sustainable energy solutions in such combustion systems. In this regard, exergy flow analyses, sometimes referred to as the second law analysis, become crucial in the evaluation of systems [20, 21]. Exergy analysis is a useful tool for increasing a system's overall efficiency because it can indicate the origins, extent, and locations of thermodynamic inefficiencies [22]. Therefore, researchers have pointed out that the second law of thermodynamics should be used to make a better evaluation of the systems they examine to reveal the destruction of exergy in the systems [23].

Terhan and Comakli [24] performed the exergy analysis of a natural gas-fuelled boiler used for district heating. They reported that the maximum exergy destruction occurred in the combustion chamber, and the exergy efficiency of the boiler was 32.77% while energy efficiency was 82.21%. Costa et al. [25] carried out an exergy analysis of a thermal power plant with a 50 MW capacity using residual forest biomass fuel. They stated that the main irreversibility occurred in the combustion chamber, and the potential for enhancing the system efficiency is by reducing the moisture content in the biomass. Zueco et al. [26] conducted the exergy analysis of a power plant using different fuels, n-octane, methane, propane, and soybean-based biodiesel. Similarly, they concluded that the main source of the exergy destruction stems from the combustion process in the boiler. Besides, it is stated that the fuel with a simple molecular structure and oxygen will reduce the exergy destruction, although exergy efficiencies were reported at about 31% for all fuels used in the study.

Along with the exergy analyses for boiler and power plant combustion systems, much research is also available on the exergy analyses on internal combustion engines for different combustion strategies and fuels [27-29]. Li et al. [30] studied the exergy analysis of three different combustion modes in internal combustion engines, namely conventional diesel combustion (CDC), homogeneous charge compression ignition (HCCI), and reactivity controlled compression ignition (RCCI). Wang et al. [31] performed an extensive study on a turbocharged hydrogen engine to map exergy efficiencies for varying engine speed and load. They reported that the hydrogen-fuelled engine is limited theoretically by 59% exergy efficiency. In general, many of these studies reported that most of the exergy loss occurs during the combustion process.

Literature survey shows that there are numerous studies performed exergy analyses of systems involving the combustion process. However, the exergy analysis of oxy-biogas combustion in a chamber is missing in the literature, which is a research gap in this field. Besides, no studies have evaluated the effect of CO_2 content on oxy-biogas combustion in terms of exergy. The current study aimed, therefore, to investigate the exergy analysis of oxy-biogas combustion in a furnace designed for natural gas system oxy-combustion presented in the study of Yin et al. [32], to reveal the effect of CO_2 content of biogas during oxy-fuel combustion considering both thermo-mechanical and chemical exergy, to determine the exergy loss due to incomplete combustion by varying CO_2 content. Thus, the current study contributes to the literature in this field by presenting findings based on exergy analyses of oxy-biogas combustion, which is a proposed strategy to overcome drawbacks, such as the lower calorific value of biogas and combustion stability encountered during the combustion process.

2. Materials and Methods

In the present work, combustion modeling of biogases consisting of different rates of CO_2 content was numerically carried out under oxy-fuel conditions in a furnace. The combustion model was simulated using the ANSYS-Fluent CFD software tool, which employs the control volume method. Thus, the combustion characteristics and exergetic investigations were performed by the simulated results. The detailed model development and exergy analysis procedure are given in the following sections.

2.1 Geometric Model and Model Formulation

A three-dimensional furnace model was created to simulate the oxy-combustion by considering the dimensions of a 0.8 MW oxy-natural gas flame furnace in the reference [32]. The furnace has a horizontal design, a square cross-section with 1.05 m x 1.05 m, and a 3.44 m length. The furnace has a burner consisting of a fuel inlet with a 16 mm diameter and two annulus having 28mm and 36mm outer diameters for air entrance. An exhaust line with a 500 mm diameter and a 740 mm length was also designed for the exhaust gas exit. The furnace was modeled in its quarter segment to reduce the computational time since the model can be defined by symmetry boundaries. Thus, the model was meshed with the hexahedral elements for the computational domain as shown in Figure 1.

The model formulations consist of conservation equations of mass, momentum, energy, and transport equations in three-dimensional cartesian coordinates. The equations were solved in the computational domain in which flow with chemical reactions takes place, to estimate the flow field, thermal, and combustion products. The conservation equations and transport equations are expressed for steady-state and Newtonian fluids as follows [33]:

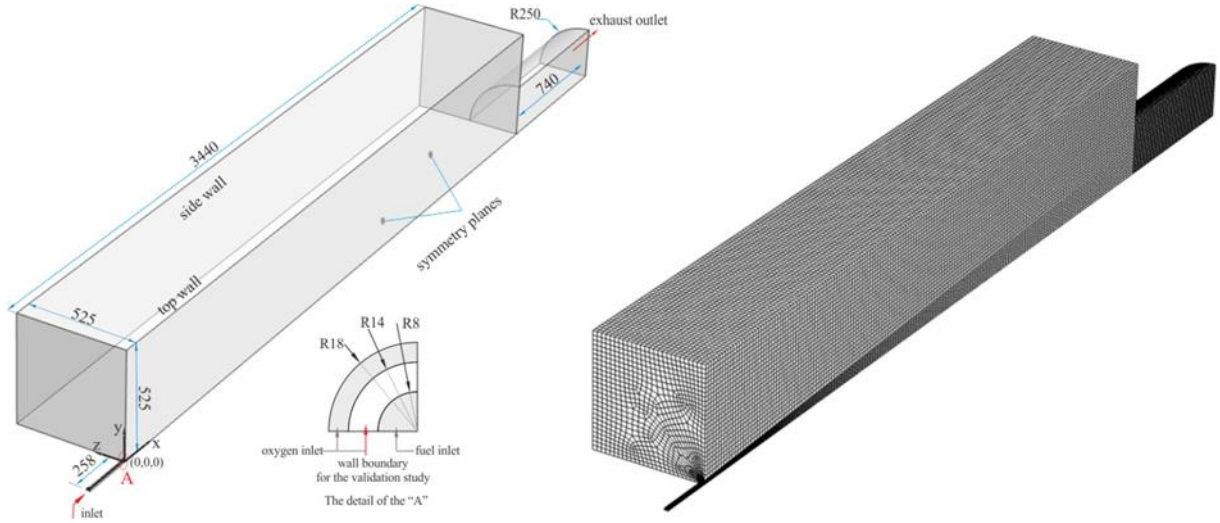

Figure 1. The modelled furnace and its grid structure.

Continuity equation

$$\nabla\left(\rho\vec{V}\right) = 0 \tag{1}$$

Momentum equation

$$\nabla\left(\rho\vec{V}\vec{V}\right) = -\nabla p + \nabla.(\tau) + \rho\vec{g} + \vec{F} \tag{2}$$

where, $\vec{V}$ is the velocity vector, ρ is the density of the fluid. In Eq. (4), p and τ represent the static pressure and stress tensor, respectively. $\vec{F}$ denotes the external body forces, and $\rho\vec{g}$ is the gravitational force.

Energy equation

$$\nabla \cdot \left[\vec{V}(\rho E + p)\right] = \nabla \cdot \left[k_{eff}\nabla T - \sum h_i\vec{J_i} + \left(\tau_{eff} \cdot \vec{\vartheta}\right)\right] + S \tag{3}$$

where, T is temperature and k_{eff} is defined as the effective conductivity. $\vec{J_i}$ is the diffusion flux of species i, E is total energy, h is sensible enthalpy, and S is the energy source due to the combustion reaction. The total energy is defined as:

$$E = h - \frac{p}{\rho} + \frac{v^2}{2} \tag{4}$$

The enthalpy for ideal gas mixture is expressed as:

$$h = \sum x_i h_i \tag{5}$$

In Eq. (5), x_i is the mass fraction of i th species in a mixture.

The mass fraction of the species in combustion reactions is determined by the species transport equations, and the conservation equation becomes in the following form [34]:

$$\nabla.\left(\rho\vec{V}x_i\right) = -\nabla.\vec{J_i} + R_i \tag{6}$$

where R_i and $\vec{J_i}$ are the net production rate and the diffusion flux of i th species in chemical reaction, $\vec{J_i}$ is defined as follows:

$$\vec{j}_i = -\left(\rho D_{i,m} + \frac{\mu_t}{Sc_t}\right)\nabla x_i \tag{7}$$

where $D_{i,m}$ represents the diffusion coefficient for species i, and Sc_t is the turbulent Schmidt number, which is set to 0.7 [35].

The present work employs the Eddy-Dissipation-Concept (EDC) model, incorporating chemical kinetic mechanisms, to determine the term R_i in Eq. (6) [36]. In the EDC model, chemical reaction occurs in small turbulent scales defined by the fine scales; the length fraction of the fine scales and the volume fraction of the fine scales. They are calculated as follows [37]:

$$\gamma^* = C_\gamma\left(\frac{\nu\epsilon}{k^2}\right)^{1/4} \tag{8}$$

where, * indicates the quantities of the fine scales. ν, ϵ, and k are the kinematic viscosity, the dissipation rate, and turbulent kinetic energy, respectively. C_γ is a time scale constant. The volume fraction of the scales is estimated as γ^{*3}. A variety of species react in the fine structures across the time scale calculated by Eq. (9).

$$\tau^* = C_\tau\left(\frac{\nu}{\epsilon}\right)^{1/2} \tag{9}$$

The C_τ is a time scale constant. The constants, C_γ and C_τ were set to 1.0 and 3.0 [38] for the current study.

The present work used the modified 4-step global combustion mechanism of Jones and Lindstedt [32, 39]. The mechanisms with Arrhenius equation parameters, which determine the related reaction rate, are given in Table 1. The Arrhenius expression is given by Eq. (10).

$$k_r = A\,T^\beta \exp\left(-\frac{E}{RT}\right) \tag{10}$$

In Eq. (10), k_r represents the reaction rate constant of reaction r. A and β are the pre-exponential factor and temperature exponent, respectively. E and R denote the activation energy for the relevant reaction and the universal gas constant, respectively

The flow field and temperature distribution in the combustion environment are essential to well predict the species since reactions occurring interact with turbulent and heat transfer mechanisms [40]. Therefore, the turbulence and radiation effects were considered by the models; the standard k-ϵ turbulence model and the P1 radiation model in the present study.

Table 1. The modified global mechanism of Jones and Lindstedt (JL_modified).

No	Reactions	Rate exponent	A	β	E [j/kmol]
R1	$CH_4 + 0.5O_2 \rightarrow CO + 2H_2$	$[CH_4]^{0.5}$ $[O_2]^{1.25}$	$4.4\ 10^{11}$	0	$1.26\ 10^{8}$
R2	$CH_4 + H_2O \rightarrow CO + 3H_2$	$[CH_4]$ $[H_2O]$	$3.0\ 10^{8}$	0	$1.26\ 10^{8}$
R3	$H_2 + 0.5O_2 \leftrightarrow H_2O$	$[H_2]$ $[O_2]^{0.5}$	$5.69\ 10^{11}$	0	$1.465\ 10^{8}$
R4	$CO + H_2O \leftrightarrow CO_2 + H_2$	[CO] $[H_2O]$	$2.75\ 10^{9}$	0	$8.36\ 10^{8}$

The standard k- ϵ model has two transport equations for the turbulence kinetic energy (k) and the dissipation rate (ϵ), which are expressed in Eq. (11) and (12) [34, 41].

$$\frac{\partial}{\partial x_i}(\rho k V_i) = \frac{\partial}{\partial x_j}\left[\left(\mu + \frac{\mu_t}{\sigma_k}\right)\frac{\partial k}{\partial x_j}\right] + G_k + G_b - \rho\epsilon - Y_M \quad (11)$$

$$\frac{\partial}{\partial x_i}(\rho\epsilon V_i) = \frac{\partial}{\partial x_j}\left[\left(\mu + \frac{\mu_t}{\sigma_\epsilon}\right)\frac{\partial \epsilon}{\partial x_j}\right] + C_{1\epsilon}\frac{\epsilon}{k}(G_k + C_{3\epsilon}G_b) - C_{2\varepsilon}\rho\frac{\epsilon^2}{k} - R_\epsilon + S_\epsilon \quad (12)$$

In Eq. (11) and (12), G_κ *and* G_b represent the turbulence kinetic energy generation due to the mean velocity gradients and buoyancy, respectively. Y_M is the component of the total dissipation rate attributed to the fluctuating dilatation. σ_κ and σ_ε denote the turbulent Prandtl numbers of k and ε, respectively. $C_{1\varepsilon}$, $C_{2\varepsilon}$, and $C_{3\varepsilon}$ are model constants.

The P-1 radiation model is expressed as in Eq. (13) for radiation flux, q_r, which can be considered in the energy equation for the heat source [34].

$$-\nabla q_r = aG - 4a\sigma T^4 \quad (13)$$

In Eq. (13), G is the incident radiation, σ is the Stefan-Boltzmann constant, and a represents the absorption coefficient.

2.2 Solving Process

The combustion model was simulated for biogas fuel under stoichiometric oxy-fuel combustion at a constant power capacity of 0.5 MW supplied from the fuel. Biogases were regarded as a mixture composed of CH_4 and CO_2 components [14, 17, 42]. The fuels used for simulation are summarized in Table 2.

Table 2. The fuel components and lower heating values.

Definition	Components (by volume)	*LHV[MJ/kg]
M60C40	60%CH_4 + 40% CO_2	17.6471
M70C30	70%CH_4 + 30% CO_2	22.9508
M80C20	80%CH_4 + 20% CO_2	29.6296
M90C10	90%CH_4 + 10% CO_2	38.2979

* The values were calculated as given in Reference [7].

Considering the fuel components and the lower heating values, the fuel mass flow rates were calculated corresponding to a power of 0.5 MW from fuel input. Thus, the oxygen mass flow rates were determined for a stoichiometric mixture for each fuel component. The pressure and temperature of the fuel and oxygen inputs are considered at atmospheric pressure and 298.15 K, respectively. Besides, the walls of the modelled furnace were subjected to adiabatic boundary conditions, meaning no heat transfer on the walls. The equations were solved with the pressure-based solver and SIMPLE algorithm scheme for pressure-velocity coupling. The second-order upwind schemes were employed for spatial discretization of the equations. Thus, the equations were solved with the convergence criteria of 10^{-7} for the energy and P1 model equations and 10^{-3} for the continuity equation and others.

With the CFD model study, temperature distribution and combustion products were attained for combustion characteristics and exergy analysis for each fuel stated in Table 2.

2.3 Exergy Analysis

Exergy analysis is critical to an assessment of the combustion process since it provides valuable insight into irreversibility and reveals potential being able to be further utilized in a thermodynamic system or process [20]. Therefore, the present work focused on the exergy evaluation of oxy-biogas combustion for different CO_2 contents. Considering the combustion system in the current study, the system is a steady-flow combustion process without exergy input/output by both heat and work. Therefore, the exergy balance equation is expressed as follows:

$$\dot{Ex}_r - \dot{Ex}_p - \dot{Ex}_d = 0 \quad (14)$$

where, *r*, *p*, and *d* indicate reactant, products, and destruction, respectively. The reactants in the combustion process are fuel and oxygen. Thus;

$$\dot{Ex}_r = \dot{m}_f ex_f + \dot{m}_{O2} ex_{O2} \quad (15)$$

where, ex_f and ex_{O2} are the specific exergy (kJ/kg) of fuel and oxygen, respectively. The $\dot{m}_f$ and $\dot{m}_{O2}$ denote the mass flow rates of fuel and oxygen in the reactant.

Similarly, the exergy of the product mixture consisting of six species (O_2, CO_2, CO, H_2O, H_2, and CH_4) in the current study is calculated by the following equation.

$$\dot{Ex}_p = \dot{m}_p ex_p \quad (16)$$

In Eq. (16), ex_p represents the specific exergy of products. The $\dot{m}_p$ is the mass flow rate of the products, which equals the sum of the mass flow rates of fuel and oxygen.

The exergy in the combustion process can be divided into two parts, thermo-mechanical exergy (ex_{tm}) and chemical exergy (ex_{ch}). Therefore, exergy expression can be written as follows:

$$ex = ex_{tm} + ex_{ch} \quad (17)$$

By eliminating the contribution of kinetic and potential energy, the specific thermo-mechanical exergy for an ideal gas can be expressed as follows [43]:

$$ex_{tm} = (h - h_0) - T_o\left(c_p ln\frac{T}{T_o} - Rln\frac{P}{P_0}\right) \quad (18)$$

where, h is the specific enthalpy of the mixture of reactants or products. c_p and R are the specific heat capacity and the gas constant, respectively. The notation "o" indicates the dead state where the system is in thermo-mechanical equilibrium with its surrounding.

The chemical exergy of an ideal gas mixture is calculated as follows [44]:

$$ex_{ch} = \frac{1}{MW_{mix}}\left(\sum y_i\, ex^{o}_{ch,i} + R_u T_o \sum y_i ln y_i\right) \quad (19)$$

where, MW_{mix} is the molecular weight of the mixture of reactants or products. y_i is the mole fraction of species i in the mixture. R_u is the universal gas constant. $ex^{o}_{ch,i}$ is the standard molar chemical exergy of the species i. The standard molar chemical exergy is calculated by considering the mole fraction of each species at the reference environment, which is presented in Table 3 [45], as given by:

$$ex^{o}_{ch,i} = -RT_o \ln\left(y_{i,o}\right) \quad (20)$$

As shown in Table 2, the mole fraction of CH_4 is not present in the reference environment. Therefore, it was determined by utilizing the formation reaction of CH_4 and the standard Gibbs free energy of the species in the reaction, as in the reference [46]. Table 3 also summarizes the calculated standard molar chemical exergy.

Table 3. The reference molar fraction of the species and its standard molar exergy.

Species	Mole Fraction ($y_{i,o}$)	Std. Molar ChemicalExergy ($ex^{o}_{ch,i}$) (kJ/mol)
N_2(g)	0.7567	0.6917
O_2(g)	0.2035	3.9465
CO_2(g)	0.000345	19.7611
CO(g)	0.000007	29.4226
H_2O(g)	0.0303	8.6675
H_2(g)	0.0000005	35.9643
CH_4(g)	-	829.9431

Thus, the exergy destruction in combustion process for each fuel was calculated using Eq. (14) as given in Eq. (21).

$$\dot{Ex}_d = \dot{Ex}_r - \dot{Ex}_p \quad (21)$$

Finally, incomplete combustion exergy loss fraction ($f_{E,ic}$) was determined as follows [47]:

$$f_{E,ic} = \frac{\dot{Ex}_{ch,p}}{\dot{Ex}_{ch,r}} x100 \quad (22)$$

where, the notations "*ch,p*", "*ch,r*" denote the chemical exergy fractions of the products (exhaust gas) and reactants in the combustion process.

2.4 Mesh Dependency

The grid structures were created meshed with hexahedral cells by considering flow characteristics and the near-wall treatment model, which is the standard wall function in the present study. Hence, adequately fine mesh structures were created in the region of fuel and air streams in which strain flows may occur. On the other hand, course mesh structures were created on the near walls of the furnace to provide $30 < y^+ < 300$ of which the near-wall model requires. To determine the grid effect on the result, the simulation was performed in different grid structures for oxy-methane combustion with the JL_modified mechanism. The effect of the grid structures is given in Table 4. Since the further increase in the cell number did not change the results considerably, the simulation in the current study was performed on the grid structure with 169605 cells.

Table 4. The effect of the grid structure on the exhaust gas parameters.

	Cell number	T_{exh} [K]	Mole Fraction			
			CO_2	CO	O_2	H_2O
Mesh1	93897	1933.487	0.3195	5.795e-6	0.0412	0.6285
Mesh2	169605	1933.399	0.3106	5.892e-6	0.0406	0.6221
Mesh3	214263	1931.824	0.3187	5.874e-6	0.0409	0.6202

3. Validation

The model was validated by comparing with the data of the temperature and velocity distribution obtained at a 0.8 MW furnace capacity with the JL_modified reaction mechanism presented by Yin et al. [32]. As in the reference, the validated simulation was carried out using the same mass flow rates of the fuel and oxygen inputs for oxy-fuel combustion. Besides, the boundary condition on the walls was subject to a varying temperature profile with respect to axial distance. Figure 2 shows the combustion temperature and x-velocity variations at 142 cm from the burner inlet. The simulation results are compatible with those of Reference 32. Thus, the simulation model can predict reliable results for the evaluation of oxy-biogas combustion.

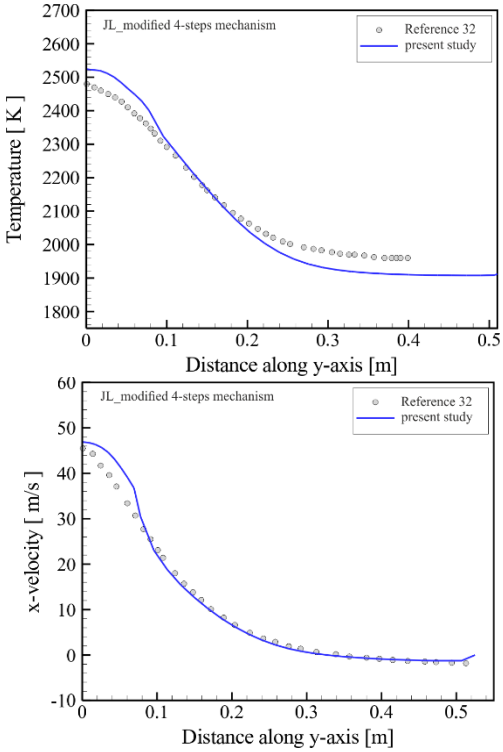

Figure 2. Comparison of the simulation results at 142 cm from the burner in the furnace with a 0.8 MW capacity.

4. Results

4.1 Temperature Development

In Figure 3, axial temperatures are given comparatively in combustion processes using M60C40, M80C20, M70C30, and M90C10 fuel types. Accordingly, it is seen that the maximum temperature is obtained with the M90C10 fuel

type. The lowest temperature was recorded in the M60C40 fuel type. It was determined that the temperature is directly proportional to the CH_4 content of the fuel and inversely proportional to the CO_2 content. This can be explained by inert gases such as CO_2 absorbing heat from the combustion process and acting as flame inhibitors. The presence of CO_2 therefore reduces the speed of the flame burning and the combustion rate (the rate at which reactants are converted to combustion products) [48].

Similarly, Sivri et al. [49] tested biogas mixtures containing different amounts of CO_2 in their study on the combustion characteristics of biogas mixtures. They found that high CO_2 concentration decreased the combustion rate and caused lower axial temperature values. Ghenai and Janajreh [50] also argued that the dilution of CH_4-containing fuels with CO_2 and nitrogen reduces the flame temperature. Furthermore, the decreases in temperature can also be attributed to the reduction in the calorific value of the fuel with the increasing CO_2 content.

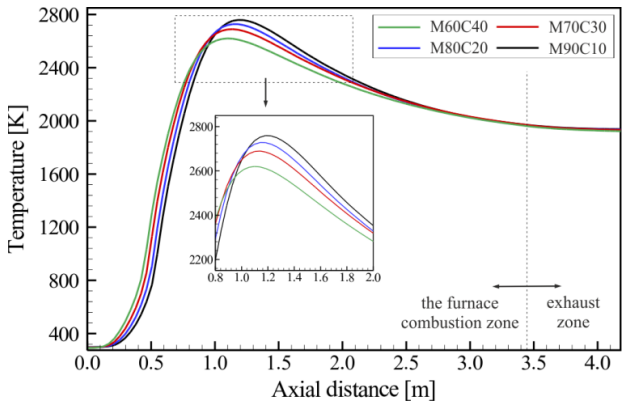

Figure 3. Comparison of the axial temperature values for different fuels.

The velocity changes along the x-axis in the combustion chamber for different fuels are given in Figure 4. Velocity profiles for the fuels show similar trends. As seen in the figure, velocity values in the combustion chamber are high at x=0.

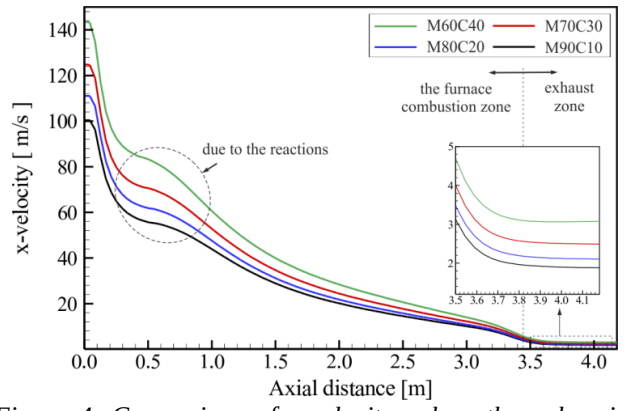

Figure 4. Comparison of x-velocity values through axial distance for different fuels.

After the fuel and oxygen entered the combustion chamber, the velocities have decreasing trends. However, the velocities partially increased between 0.5 m and 1.0 m of the axial distance due to the reaction heat. Afterward, the velocity values along the axis slowed down as the effect of the reaction heat decreased and exited the exhaust region with low velocities. Comparing the velocity values, the velocity values in the case of M60C40 fuel are the highest among the others, and the velocity values decrease with decreasing CO_2 content of biogas. This is due to a decrease in mass flow rate at the same furnace capacity (see Table 5).

Figure 5 illustrates the temperature distributions along the y-axis at x=1.1 m, where the maximum axial temperature occurs approximately (see Figure 3). It is observed that the axial temperature distribution increases with the decrease of the CO_2 ratio in the fuel. Therefore, the highest temperature values were obtained in the M90C10 fuel, while the lowest were in the M60C40 fuel. The reaction zones have high-temperature gradients [51]. Therefore, it can be stated that the change in temperature values after roughly y=0.3 m remains nearly constant, which corresponds to the flame radius at the x=1.1 m.

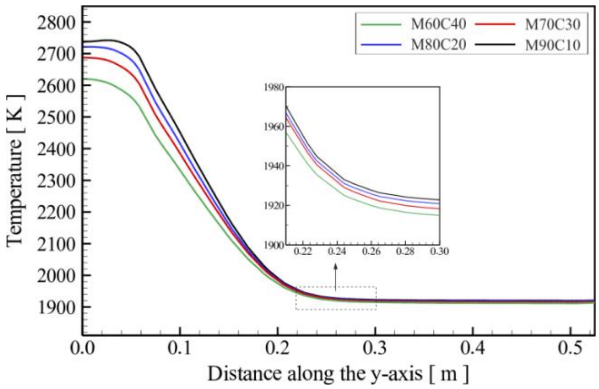

Figure 5. Comparison of temperature values with the y- axis at x=1.1 m.

Figure 6 shows the x-velocity variations in the y-axis direction at the x=1.1 m point for each fuel. As shown in the figure, the velocities are the highest in the center of the combustion chamber due to the highest flame temperature. The x-velocities decrease away from the center of the combustion chamber due to the decreasing or completing reactions, as compatible with the trends in temperature variation given in Figure 5.

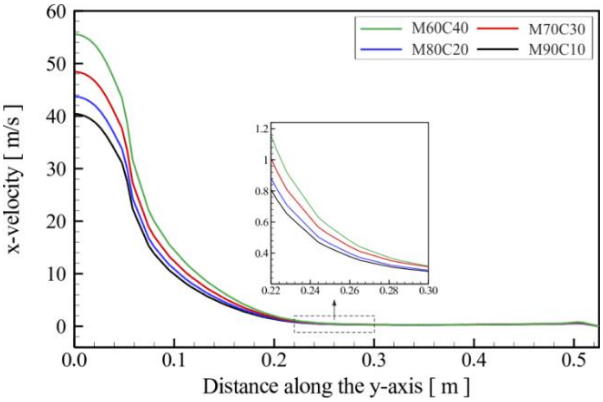

Figure 6. Comparison of x-velocity values with the y-axis at x=1.1 m.

Furthermore, the velocity gradients with the y-axis are nearly zero after x=0.3 m, which is similar to temperature variations. Generally, it is seen that the highest velocity profile belongs to M60C40 fuel. As mentioned above, the mass flow rate at the same furnace capacity gets bigger with the increasing CO_2 content of biogas, which elevates the velocity values.

Figure 7 illustrates the obtained maximum temperature values in the combustion zone and the exhaust temperature variation versus CO_2 content in biogas. It is seen that the increasing CO_2 content brings about a decrease in both the maximum temperature and exhaust temperature. The increasing carbon dioxide with high heat capacity gives rise to decreasing combustion temperature, which in turn decreases the average exhaust temperature [52]. The maximum temperature values were obtained from about 2765 K to 2625 K by varying the CO_2 content. Besides, the exhaust temperatures varied between 1926 K and 1938 K, meaning the average temperature drop is approximately 12 K between M90C10 and M60C40 fuels. A similar trend in the drop in exhaust temperature at a constant power was reported by Bastani et al. [53].

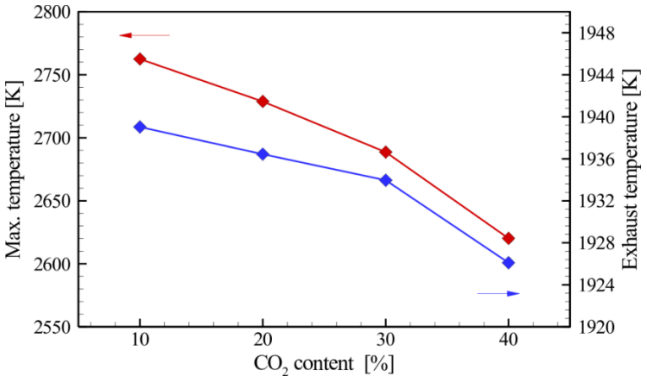

Figure 7. The variation of maximum temperature and exhaust temperature with CO_2 content in biogas.

4.2 Exergetic Evaluation

The section is dedicated to presenting the exergy analysis results. As stated in Section 2.3, the combustion chamber exergy input is provided by reactants consisting of biogas and oxygen at atmospheric pressure and ambient temperature. Therefore, the part of its chemical exergy is only considered by neglecting thermo-mechanical exergy. The calculated specific exergy and exergy flow rates are presented in Table 5 for each fuel. As expected, the maximum specific exergy belongs to M90C10 since it has the highest concentration of CH_4 which has a higher standard molar chemical exergy than that of CO_2 (see Table 3).

Table 5. The specific exergy values and exergy flow rates of the reactants for the fuels.

Fuels	Specific Exergy [kJ/kg]		Mass Flow Rate [kg/s]		Exergy Flow Rate [kW]
	ex_f	ex_{o2}	$\dot{m}_f$	$\dot{m}_{O2}$	$\dot{Ex}_r$
M90C10	39793.5680	123.3281	0.0131	0.04	524.4602
M80C20	30864.1802		0.0169		525.7661
M70C30	23990.7491		0.0218		527.5887
M60C40	18536.8392		0.0283		530.1435

Besides, the exergy flow rates for each fuel are calculated by the sum of the exergy flow rates of the fuels and oxygen as given in Eq. (15). As shown in the table, the exergy flow rates of the reactant relatively increase by increasing CO_2 content due to the increasing mass flow rate calculated by considering the same energy flow rate, 0.5 MW.

Generally, exergy values of fuels are determined by multiplying the lower heating value of fuel (LHV) and the coefficient ϕ which is the ratio of the specific exergy to the lower heating value and calculated depending on the related fuel content [54]. Similar manner, the correlation developed in the current study for biogas fuel for different CO_2 contents (f_{co2} -by volume) is presented below:

$$0 < f_{co2} \leq 0.4$$
$$\phi = 1.0374 + 0.056012(f_{co2})^{1.60193}$$
$$ex_{f,biogas} = \phi x LHV \quad (23)$$

The exergy of the exhaust gases was determined by considering the exhaust gas temperature values (given in Figure 7) and combustion products for each fuel. The obtained mass fractions of each species are given in Table 6. The specific exergy values of the exhaust gas are illustrated in Figure 8. M90C10 shows the highest specific exergy value by 6753.6 kJ/kg, consisting of 91.7 % thermo-mechanical exergy part and 8.3 % chemical exergy. On the other hand, the lowest specific exergy of the exhaust gas was attained at M60C40 by 5985.5 kJ/kg, including 82.3 % thermo-mechanical exergy and 17.7 % chemical exergy fractions.

Table 6. Mass fraction of the combustion products.

Fuels	Species					
	CO_2	CO	H_2O	H_2	O_2	CH_4
M90C10	0.5857	1.44e-5	0.4027	0.0099	0.00121	0.00051
M80C20	0.6064	1.56e-5	0.3767	0.0153	0.00096	0.00063
M70C30	0.6260	1.95e-5	0.3474	0.0247	0.00089	0.00091
M60C40	0.6407	2.91e-5	0.3189	0.0379	0.00077	0.00164

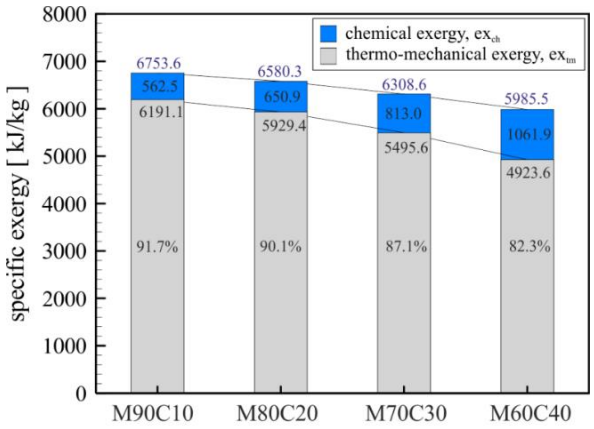

Figure 8. The specific exergy values of exhaust gas mixtures.

Figure 9 shows the exergy flow rates in the furnace. As understood in the figure, the highest exergy destruction ($\dot{Ex}_d$) occurred in M90C10 fuel with 166.14 kW, while the lowest is in M60C40 with 121.14 kW.

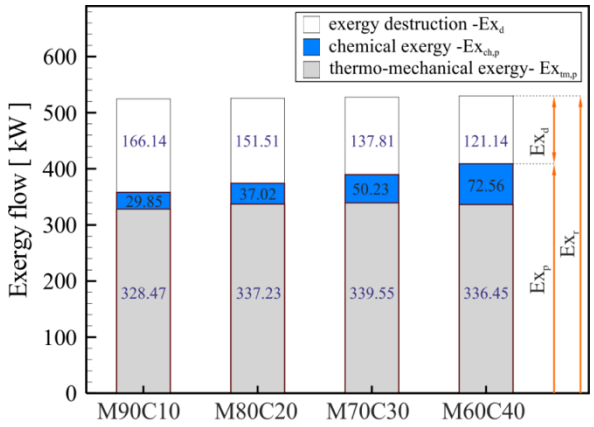

Figure 9. Exergy flow rates for biogas combustion with varying CO_2 content in the furnace.

As a general result, the reduction of CO_2 in biogas causes an increase in the exergy destruction flow in the current combustion system. Another significant result is that the chemical exergy flow of exhaust gas ($\dot{E}x_{ch,p}$) rises with increasing CO_2 content in biogas. Therefore, the chemical exergy flow in the exhaust reached 72.56 kW in the case of M60C40.

The chemical exergy flow in the exhaust gives an insight into the incomplete combustion exergy loss. Therefore, the chemical exergy flow fractions due to incomplete combustion ($f_{E,ic}$) are shown in Figure 10 for different CO_2 contents. As can be seen, the increasing CO_2 concentration influences considerable incomplete combustion, and the $f_{E,ic}$ value reached about 13.8 % at 40 % CO_2 content (M60C40) while it is about 5.8 % at 10 % CO_2 (M90C10).

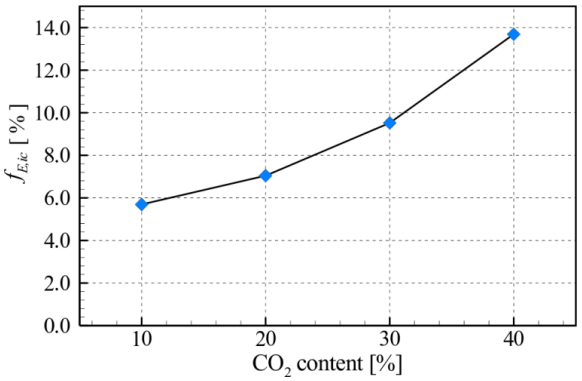

Figure 10. Exergy loss ratio due to incomplete combustion, $f_{e,ic}$.

5. Conclusion

This study investigates the exergy analysis of oxy-biogas combustion in the furnace with a 0.5 MW input power capacity and the adiabatic condition. The focus is on how the varied biogas content with CO_2 ratio influences the exergy flow rates involving thermo-mechanical exergy and chemical exergy. Therefore, the specific exergy and exergy flow rates of reactants and products in the combustion process were calculated for each biogas content varying from 10% CO_2 to 40% CO_2 with a 10% increment, and the obtained results were compared to each other. Additionally, the exergy loss ratios due to incomplete combustion were evaluated considering the chemical exergy flow in the exhaust.

The main findings based on the results are the following:

- The increasing CO_2 concentration in biogas reduced the maximum temperature values in the combustion zone due to its high heat capacity and lowering O_2 concentrations in reaction zones.
- Lowering calorific values with the increase in CO_2 in biogas led to an increase in the mass flow rates to maintain the input power constant, which resulted in the increasing exergy flow rates of the reactants.
- With increasing CO_2 content, the specific exergy of the combustion products decreased while the exergy flow rates increased due to the mass flow rates.
- The chemical exergy fractions of the combustion products increased with elevating CO_2 content in biogas, and the chemical exergy fraction was found to be 17.7% in biogas with 40% CO_2 content while 8.3% at 10% CO_2 content.
- The exergy destruction decreased with increasing CO_2 content in biogas in the current combustion system
- The increasing CO_2 gave rise to an increase in the exergy loss due to incomplete combustion. Thus, the exergy loss fraction due to incomplete combustion was found to be 13.8% in biogas with 40% CO_2 while 5.8% at 10% CO_2 content.

It should be mentioned that one possible limitation of the study is related to the EDC model constant values. These values may differ somewhat depending on the mixture properties in the combustion chamber, which may cause uncertainties in the findings. For future work, further analysis can be performed with different burner and combustion chamber designs, which are also significant factors along with fuel content. These attempts are needed to establish more efficient combustion systems for sustainability.

References:

[1] C. M. Plugge, "Biogas," *Microbial Biotechnology*, vol. 10, no. 5, pp. 1128-1130, Sep. 2017, doi: 10.1111/1751-7915.12854.

[2] N. Scarlat, J. -F. Dallemand, and F. Fahl, "Biogas: Developments and perspectives in Europe," *Renewable Energy*, vol. 129, pp. 457-472, Dec. 2018, doi: 10.1016/j.renene.2018.03.006.

[3] S. Rasi, A. Veijanen, and J. Rintala, "Trace compounds of biogas from different biogas production plants," *Energy*, vol. 32, no. 8, pp. 1375-1380, Aug. 2007, doi: 10.1016/j.energy.2006.10.018.

[4] A. Rafiee, K. R. Khalilpour, J. Prest, and I. Skryabin, "Biogas as an energy vector," *Biomass and Bioenergy*, vol 144, Jan. 2021, Art. no. 105935, doi: 10.1016/j. biombioe.2020.105935.

[5] S. E. Hosseini and M. A. Wahid, "Development of biogas combustion in combined heat and power generation," *Renewable and Sustainable Energy Reviews*, vol. 40, pp. 868-875, Dec. 2014, doi: 10.1016/j.rser.2014.07.204.

[6] S. E. Hosseini, G. Bagheri, and M. A. Wahid, "Numerical investigation of biogas flameless combustion," *Energy Conversion and Management*, vol. 81, pp. 41-50, May 2014, doi: 10.1016/j.enconman. 2014.02.006.

[7] M. Yıldız, "Chemical equilibrium based combustion model to evaluate the effects of H2 addition to biogases with different CO2 contents," *International Journal of Hydrogen Energy*, vol. 52, pp. 1334-1344, Jan. 2024, doi: 10.1016/j.ijhydene.2023.06.077.

[8] J. P. Gómez Montoya, A. A. Amell, and D. B. Olsen, "Prediction and measurement of the critical compression ratio and methane number for blends of biogas with methane, propane and hydrogen," *Fuel*, vol. 186, pp. 168-175, Dec. 2016, doi: 10.1016/j.fuel.2016 .08.064.

[9] S. Benaissa, B. Adouane, S. M. Ali, S. S. Rashwan, and Z. Aouachria, "Investigation on combustion characteristics and emissions of biogas/hydrogen blends in gas turbine combustors," *Thermal Science and Engineering Progress*, vol. 27, Jan. 2022, Art. no.

101178, doi: 10.1016/j.tsep.2021.101178.

[10] A. Sharma, Y. Singh, N. Ahmet Ansari, A. Pal, and S. Lalhriatpuia, "Experimental investigation of the behaviour of a DI diesel engine fuelled with biodiesel/diesel blends having effect of raw biogas at different operating responses," *Fuel*, vol. 279, 2020, Art. no. 118460, doi: 10.1016/j.fuel.2020.118460.

[11] M. Sekar, M. YE. Selim, and M. Elgendi, "Improving the performance of a diesel engine using nanomaterials and chlorella vulgaris microalgae blends assisted with biogas," *International Journal of Hydrogen Energy*, vol. 49, pp. 496-506, Jan. 2024, doi: 10.1016/j.ijhydene. 2023.09.171.

[12] İ. Yilmaz, B. Alabaş, M. Taştan, and G. Tunç, "Effect of oxygen enrichment on the flame stability and emissions during biogas combustion: An experimental study," *Fuel*, vol. 280, Nov. 2020, Art. no. 118703, doi: 10.1016/j.fuel.2020.118703.

[13] K. Safer, M. Safer, F. Tabet, and A. Ouadha, "A numerical investigation of oxygen-enriched biogas counter-flow diffusion flames," *Combustion Science and Technology*, vol. 196, no. 8, pp. 1207-1226, Jun. 2024, doi: 10.1080/00102202.2022.2112955.

[14] K. Cacua, A. Amell, and F. Cadavid, "Effects of oxygen enriched air on the operation and performance of a diesel-biogas dual fuel engine," *Biomass and Bioenergy*, vol. 45, pp. 159-167, Oct. 2012, doi: 10.1016/j.biombioe.2012.06.003.

[15] H. A. Alabaş and B. Albayrak Çeper, "Effect of oxygen enrichment on the combustion characteristic and pollutant emissions of kerosene-biogas mixtures on a mini jet engine combustion chamber," *Journal of the Energy Institute*, vol. 111, Dec. 2023, Art. no. 101420, doi: 10.1016/j.joei.2023.101420.

[16] X. Wang et al., "Effect of propane addition and oxygen enrichment on the flame characteristics of biogas," *Energy & Fuels*, vol. 35, no. 6, pp. 5015-5025, Mar. 2021, doi: 10.1021/acs.energyfuels.1c00113.

[17] B. Alabaş, G. Tunç, M. Taştan, and İ. Yilmaz, "Effect of oxygen enrichment of Biogas-Hydrogen mixtures in a premixed combustor on the combustion instability and emissions," *Fuel*, vol. 340, May 2023, Art. no. 127498, doi: 10.1016/j.fuel.2023.127498.

[18] J. Li et al., "Combustion and heat release characteristics of biogas under hydrogen-and oxygen-enriched condition," *Energies (Basel)*, vol. 10, no. 8, p. 1200, 2017, doi: 10.3390/en10081200.

[19] N. Striūgas, R. Paulauskas, R. Skvorčinskienė, and A. Lisauskas, "Investigation of waste biogas flame stability under oxygen or hydrogen-enriched conditions," *Energies (Basel)*, vol. 13, no. 18, pp. 4760, Sep. 2020, doi: 10.3390/en13184760.

[20] M. Elwardany, "Enhancing steam boiler efficiency through comprehensive energy and exergy analysis: A review," *Process Safety and Environmental Protection*, vol. 184, pp. 1222-1250, Apr. 2024, doi: 10.1016/j.psep .2024.01.102.

[21] M. Parvez, T. Ahamad, S. Lal, O. Khan, F. Khalid, and Z. Yahya, "Energy, Exergy, Economic, and environmental assessment of a trigeneration system for combined power, cooling, and water desalination system driven by solar energy," *International Journal of Thermofluids*, vol. 22, May 2024, Art. no. 100694, doi: 10.1016/j.ijft.2024.100694.

[22] J. Galindo, S. Ruiz, V. Dolz, and L. Royo-Pascual, "Advanced exergy analysis for a bottoming organic rankine cycle coupled to an internal combustion engine," *Energy Conversion and Management*, vol. 126, pp. 217-227, Oct. 2016, doi: 10.1016/j.enconman. 2016.07.080.

[23] D.-C. Sue and C.-C. Chuang, "Engineering design and exergy analyses for combustion gas turbine based power generation system," *Energy*, vol. 29, no. 8, pp. 1183-1205, Jun. 2004, doi: 10.1016/j.energy.2004.02. 027.

[24] M. Terhan and K. Comakli, "Energy and exergy analyses of natural gas-fired boilers in a district heating system," *Applied Thermal Engineering*, vol. 121, pp. 380-387, Jul. 2017, doi: 10.1016/j.applthermaleng. 2017.04.091.

[25] V. A. F. Costa, L.A.C. Tarelho, and A. Sobrinho, "Mass, energy and exergy analysis of a biomass boiler: A portuguese representative case of the pulp and paper industry," *Applied Thermal Engineering*, vol. 152, pp. 350-361, Apr. 2019, doi: 10.1016/j.applthermaleng. 2019.01.033.

[26] J. Zueco, D. López-Asensio, F.J. Fernández, and L. M. López-González, "Exergy analysis of a steam-turbine power plant using thermocombustion," *Applied Thermal Engineering*, vol. 180, Nov. 2020, Art. no. 115812, doi: 10.1016/j.applthermaleng.2020.115812.

[27] H. Mahabadipour, S. R. Krishnan, and K. K. Srinivasan, "Investigation of exhaust flow and exergy fluctuations in a diesel engine," *Applied Thermal Engineering*, vol. 147, pp. 856-865, Jan. 2019, doi: 10.1016/j.applthermal eng.2018.10.109.

[28] M. N. Nabi and M.G.Rasul, "Influence of second generation biodiesel on engine performance, emissions, energy and exergy parameters," *Energy Conversion and Management*, vol. 169, pp. 326-333, Aug. 2018, doi: 10.1016/j.enconman.2018.05.066.

[29] S. Sarıkoç, İ. Örs, and S. Ünalan, "An experimental study on energy-exergy analysis and sustainability index in a diesel engine with direct injection diesel-biodiesel-butanol fuel blends," *Fuel*, vol. 268, May 2020, Art. no. 117321, doi:10.1016/j.fuel.2020.117321.

[30] Y. Li, M. Jia, Y. Chang, S. L. Kokjohn, and R. D. Reitz, "Thermodynamic energy and exergy analysis of three different engine combustion regimes," *Applied Energy*, vol. 180, pp. 849-858, Oct. 2016, doi: 10.1016/j.apenergy.2016.08.038.

[31] X. Wang, B. Sun, and Q. Luo, "Energy and exergy analysis of a turbocharged hydrogen internal combustion engine," *International Journal of Hydrogen Energy*, vol. 44, no. 11, pp. 5551-5563, Feb. 2019, doi: 10.1016/j.ijhydene.2018.10.047.

[32] C. Yin, L. A. Rosendahl, S. K. Kær, "Chemistry and radiation in oxy-fuel combustion: a computational fluid

dynamic modeling study," *Fuel*, vol. 90, no. 7, pp. 2519-2529, Jul. 2011, doi: 10.1016/j.fuel.2011.03.023.

[33] Wardach-Święcicka, S. Polesek-Karczewska, and D. Kardaś, "Biomass Combustion in the Helically Coiled Domestic Boiler Combined with the Equilibrium/Chemical Kinetics CFD Approach," *Applied Mechanics*, vol. 4, no. 2, pp. 779-802, Jun. 2023, doi: 10.3390/applmech4020040.

[34] Fluent User's Guide, *Centerra Resource Park,10. Cavendish Court, Lebanon, NH 03766, USA.*

[35] M. A. Nemitallah and M. A. Habib, "Experimental and numerical investigations of an atmospheric diffusion oxy-combustion flame in a gas turbine model combustor," *Applied Energy*, vol. 111, pp. 401-415, Nov. 2013, doi: 10.1016/j.apenergy.2013.05.027.

[36] M. Farokhi and M. Birouk, "Application of Eddy dissipation concept for modeling biomass combustion, Part 1: Assessment of the model coefficients," *Energy & Fuels*, vol. 30, no. 12, pp. 10789-10799, Dec. 2016, doi: 10.1021/acs.energyfuels.6b01947.

[37] E.-M. Wartha, M. Bösenhofer, and M. Harasek, "Characteristic chemical time scales for reactive flow modeling," *Combustion Science and Technology*, vol. 193, no. 16, pp. 2807-2832, Dec. 2021, doi: 10.1080/00102202.2020.1760257.

[38] M. J. Evans, P.R. Medwell, and Z.F. Tian, "Modeling lifted jet flames in a heated coflow using an optimized eddy dissipation concept model," *Combustion Science and Technology*, vol. 187, no. 7, pp. 1093-1109, Jul. 2015, doi: 10.1080/00102202.2014.1002836.

[39] J. P. Kim, U. Schnell, and G. Scheffknecht, "Comparison of different global reaction mechanisms for MILD combustion of natural gas," *Combustion Science and Technology*, vol. 180, no. 4, pp. 565-592, Feb. 2008, doi: 10.1080/00102200701838735.

[40] S. Mazumder, and S. P. Roy, "Modeling thermal radiation in combustion environments: progress and challenges," *Energies (Basel)*, vol. 16, no. 10, p. 4250, May 2023, doi: 10.3390/en16104250.

[41] J. Gorman, S. Bhattacharyya, L. Cheng, and J. P. Abraham, "Turbulence models commonly used in CFD," in *Applications of Computational Fluid Dynamics Simulation and Modeling*: IntechOpen, 2021, doi: 10.5772/intechopen.99784.

[42] C. A. Cardona and A. A. Amell, "Laminar burning velocity and interchangeability analysis of biogas/C_3H_8/H_2 with normal and oxygen-enriched air," *International Journal of Hydrogen Energy*, vol. 38, no. 19, pp. 7994-8001, Jun. 2013, doi: 10.1016/j.ijhydene. 2013.04.094.

[43] M. A. Boles, Y. A. Cengel, Thermodynamics: an engineering approach, 8 th ed. New York: McGraw-Hill Education, 2014.

[44] Y. Kalinci, A. Hepbasli, and I. Dincer, "Exergoeconomic analysis and performance assessment of hydrogen and power production using different gasification systems," *Fuel*, vol. 102, pp. 187-198, Dec. 2012, doi: 10.1016/j.fuel.2012.06.040.

[45] H. Caliskan, M. E. Tat, and A. Hepbasli, "Performance assessment of an internal combustion engine at varying dead (reference) state temperatures," *Applied Thermal Engineering*, vol. 29, no. 16, pp. 3431-3436, Nov. 2009, doi: 10.1016/j.applthermaleng.2009.05.021.

[46] R. Pal, "Chemical exergy of ideal and non-ideal gas mixtures and liquid solutions with applications," *International Journal of Mechanical Engineering Education*, vol. 47, no. 1, pp. 44-72, Jan. 2019, doi: 10.1177/030641901774958.

[47] D. Liu et al., "Theoretical analysis on the exergy destruction mechanisms and reduction under LTC relevant conditions," *Proceedings of the Combustion Institute*, vol. 37, no. 4, pp. 4797-4804, 2019, doi: 10.1016/j.proci.2018.08.012.

[48] O. Razbani, N. Mirzamohammad, and M. Assadi, "Literature review and road map for using biogas in internal combustion engines," in *3 th Int. Conference on Applied Energy*, Perugia, Italy, 2011.

[49] I. Sivri, H. Yilmaz, O. Cam, and I. Yilmaz, "Combustion and emission characteristics of premixed biogas mixtures: An experimental study," *International Journal of Hydrogen Energy*, vol. 47, no. 24, pp. 12377-12392, Mar. 2022, doi: 10.1016/j.ijhydene.2021 .08.119.

[50] C. Ghenai and I. Janajreh, "Combustion of renewable biogas fuels," *Journal of Energy and Power Engineering*, vol. 9, no. 10, pp. 831-843, 2015, doi:10.17265/19348975/2015.010.001.

[51] S. K. Som and A. Datta, "Thermodynamic irreversibilities and exergy balance in combustion processes," *Progress in Energy and Combustion science*, vol. 34, no. 3, pp. 351-376, June 2008, doi: 10.1016/j.pecs.2007.09.001.

[52] X. Tian, J. Yang, Y. Gong, Q. Guo, X. Wang, and G. Yu, "Experimental study on OH*, CH*, and CO_2* chemiluminescence diagnosis of CH_4/O_2 diffusion flame with CO_2-diluted fuel," *ACS Omega*, vol. 7, no. 45, pp. 41137-41146, Nov. 2022, doi: 10.1021/acsomega.2c04689.

[53] M. Bastani, S. Tabejamaat, M. Mani, and H. Ashini, "Numerical and experimental investigation of microturbine combustion chamber performance and emissions through biogas consumption with varied component ratios," *Fuel*, vol. 380, Jan. 2025, Art. no. 133234, doi: 10.1016/j.fuel.2024.133234.

[54] T.J. Kotas, Y.R. Mayhew, and R.C. Raichura, "Nomenclature for exergy analysis," *Proceedings of the Institution of Mechanical Engineers, Part A: Journal of Power and Energy*, vol. 209, no. 4, pp. 275-280, Nov. 1995, doi: 10.1243/PIME_PROC_1995_209_006_01.